# The Design and Flight Testing of a Long Endurance RPV

**Shahid Siddiqi & Teck-Seng Kwa**

**AS&M Inc., 107 Research Drive, Hampton, Virginia 23666, USA**

## Nomenclature

| | | | |
|---|---|---|---|
| a | lift curve slope | NLF | natural laminar flow |
| ac | aerodynamic center | RPV | Remotely Piloted Vehicle |
| $AR$ | aspect ratio | $R_c$ | chord Reynolds number |
| b | span | $R_u$ | unit Reynolds number |
| c | chord | S | wing planform reference area |
| cg | center of gravity | SM | static margin |
| $C_d$ | section drag coefficient | V | flight speed |
| $C_l$ | section lift coefficient | W | weight |
| $C_m$ | section moment coefficient | $\alpha$ | angle of attack |
| $C_D$ | drag coefficient | $\beta$ | sideslip angle |
| $C_{Di}$ | induced drag coefficient | $\Gamma_o$ | center span circulation |
| $C_L$ | lift coefficient | $\mu$ | microns, $10^{-6}$ *metres* |
| $C_M$ | moment coefficient | | |
| $e$ | Oswald efficiency factor | | *Subscripts*: |
| LRN | low Reynolds number | $c$ | canard |
| $n$ | flight load factor | $f$ | flap |
| NASA LaRC | NASA Langley Research Center | max | maximum |
| | | $t$ | horizontal tail |

## ABSTRACT

This paper covers the design process for a long endurance Remotely Piloted Vehicle. The 56 *pound* RPV must operate in the 25 – 50 *knot* speed range at low altitudes. An airfoil designed for LRN applications was used with a wing of $AR = 22$ to reach an estimated $\frac{L}{D}|_{max}$ of 25. Wing tip feathers were designed to reduce the induced drag. A comparison between the computed aerodynamic predictions and wind-tunnel results is given. The estimated endurance is on the order of 50 *hours/gallon* of fuel. A three surface configuration was chosen and the predicted handling quality and performance results obtained so far are given. The structural challenges in building a light weight structure for the wing and control surfaces are outlined. The flight test program is currently underway.

## I LRN RPV DESIGN

The principal problem faced in LRN RPV design is the drag penalty associated with laminar separation. Nonlinear and unsteady aerodynamic characteristics that occur with the laminar separation bubble phenomenon pose handling qualities problems and make performance prediction unreliable. The aerodynamic problems associated with LRN RPV's are extensively discussed in an excellent survey by [Carmichael 1981] and also by [Mueller 1985].

The overall aerodynamic design process for the high $\frac{L}{D}$ RPV can be outlined as follows. The LRN optimized airfoil selected has a two dimensional $\frac{L}{D}|_{max}$ of approximately 115 for $R_c$=250,000 (see Section III). A wing with this airfoil will then have a $\frac{L}{D}|_{max}$ of approximately 57. Wind-tunnel measurements for the fuselage gave a minimum $C_D$=.01 referenced to the wing area. These tests also showed that the unfaired landing gear $C_D$ is approximately half that of the fuselage. Typical horizontal and vertical tails can be assumed to be 40% of $S$, their $C_D$ is then .0093, assuming flow without separation for $R_c$=150,000 (which is possible with the use of turbulators, see Section III). The overall $\frac{L}{D}|_{max}$ possible for such a configuration then is approximately 27. Trim, separation and interference drag and the loss of wing planform efficiency will reduce the overall $\frac{L}{D}$ further. The design challenge is then to get an $\frac{L}{D}|_{max}$ as close to 27 as possible.

The design, wind-tunnel testing, and flight testing of a recent RPV was reported in [Stollery et al. 1988]. The project included a wind tunnel evaluation of several different airfoil sections from which the Wortmann FX63-137 was chosen. This RPV was designed to function in the $R_c$ range of 300,000 – $1\times10^6$ and used a wing $AR$ of 8 and achieved an in-flight $\frac{L}{D}|_{max}$ of 10. Older RPVs such as the Mastiff, the Aquila, etc., were not aerodynamically optimized and their estimated $\frac{L}{D}|_{max}$ is on the order of 8.

Two useful papers on composite model building techniques are available, the first is [Vranas 1984], from the NASA LaRC, which discusses molding techniques with the use of vacuum bagging. The second is [Jacob et al. 1984], from the Aeronautical Development Establishment in India, which discusses molding techniques using pressure forming. Information on existing RPVs can be found in Jane's All The World Aircraft.

## II THE LAURA PROJECT

The aim of the low altitude unmanned research aircraft (*LAURA*) research project is to investigate and flight test the potential of LRN aerodynamic technology for improving the configuration $\frac{L}{D}$. The study was sponsored by the NRL and the ONR with the participation of other government agencies and the aeronautical industry. The details of the LAURA project are reported in [Foch 1986] and [Foch & Wyatt 1986]. Standard fuselages, engines, propellers, and landing gear are used to which the different wing and control surface configurations are fitted. The design specifications for the LAURA are given in Table I. Figure 1 shows a photograph of the RPV that was built.

The four aircraft configurations being evaluated are:

- ACA Industries - joined wing
- Advanced Aeromechanisms Corp. - hinged wing
- Locus - tandem wing
- NASA/AS&M - three surface.

The initial sizing process for the LAURA mission gave the following:

[1] The wing area was sized for the required sea level, long endurance $\frac{L}{D}|_{max}$ capability. The specified speed of $V=25\,knots$ gives $S=22ft^2$ at a $C_L=1.2$.

[2] The 3-hp engine selected gives sufficient power for the high speed capability. A power of approximately 2.3 hp is required for $V = 50\,knots$ at a $\frac{L}{D} = 6$ with a propeller efficiency of approximately 50%.

[3] The 400 fpm climb requirement is easily met with this available power. A climb rate of approximately $500\,fpm$ can be obtained at $V=30\,knots$ assuming an $\frac{L}{D} = 15$.

## III AERODYNAMICS

Custom-designed airfoils for the mission requirement are the key aerodynamic factor which can assure efficient RPVs. The long endurance mission requires a high $\frac{L}{D}|_{max}$ for $C_L$'s as high as 1.2. The RPV performance goals for this design were to fly efficiently in the 25–50 *knots* speed range ($R_u$ = 250,000 – 500,000). An airfoil meeting these performance specifications was selected from a series of LRN NLF airfoils designed by Dr. Werner Pfenninger.

For low Reynolds numbers, the laminar boundary layer on the airfoil tends to be very stable and transition is not easily triggered. The inevitable adverse pressure gradient following the minimum pressure peak over an airfoil will then cause laminar separation. Conventional airfoils exhibit rapid deterioration in their aerodynamic characteristics at low chord Reynolds numbers, especially below 500,000 because of laminar separation. A good experimental investigation of the laminar separation bubble for airfoils is reported in [O'Meara & Mueller 1987]. The nonlinear effects of laminar separation can occur even at Reynolds numbers greater than a million and can be seen from the wind-tunnel measurements given in [Ferris et al. 1987] for the NASA LS(1)-0013 airfoil. Wind-tunnel measurements made with the standard NACA 0012 airfoil, in which the Mach Number and the $R_c$ were varied independently, also exhibited laminar separation characteristics. These results are reported in [Ladson 1984].

The ASM-LRN-010 airfoil was chosen for the wing; its design is discussed in [Pfenninger et al. 1988]. It was specifically designed for the LRN flight regime typical for LAURA applications ($100{,}000 < R_c < 500{,}000$). Figure 2 shows the airfoil which is a 9.5% thick airfoil with its maximum thickness located at 37%$c$. [Pfenninger & Vemuru 1988] discuss the LRN airfoil design process and give computed results for some of their airfoils. The design of this class of airfoils was based on the ideas described in [Pfenninger 1947 & 1956], and originated with the NASA LRN(1)-1007 airfoil designed to operate with high lift-to-drag ratios, near a $C_L$ of about 1.0. This is a 7.3% thick airfoil and its design details are reported in [Mangalam & Pfenninger 1984] and [Mangalam et al. 1986]. The NASA LRN(1)-1010 airfoil was chosen for the canard; this is a 9.8% thick airfoil with its maximum thickness located at 41%$c$ and its design details are reported in [Evangelista 1987].

The airfoil choice for the wing can be evaluated with respect to other available LRN airfoils on the basis of the figure of merit formula for wing endurance ($FOM_e$), given in [Maughmer & Sommers 1988], which is $FOM_e = \frac{C_{L_{max}}}{C_D @ C_{Lop}}$, where $C_{L_{op}}$ is the operational $C_L$. The $FOM_e$ comparisons are shown in Table II and were made using WT data where available or with computational predictions. Clearly the ASM-LRN-010, with $FOM_e = 115$, has the highest $FOM_e$ of the airfoils listed and hence its choice for the wing. There was no wind-tunnel data for the ASM-LRN-010, hence the NASA-LRN-1010 was chosen for the canard instead because the authors had conducted wind-tunnel tests with this airfoil down to a $R_c$ of 100,000. Many LRN airfoils have been compared in [Carmichael 1981], while [Selig et al. 1989] recently published an evaluation of 60 LRN airfoils by measuring their performance in standard wind-tunnel tests. Neither of these reports identified any airfoil which had a $FOM_e$ as high as that of the ASM-LRN-010.

Pfenninger proposed design remedies which avoid the drag penalties caused by laminar separation by forcing transition to occur just before the point where laminar separation would start thus preventing separation. The skin-friction drag is then minimized by ensuring the maximum possible extent of laminar flow without prematurely forcing transition to avoid laminar separation. To minimize drag without penalizing lift, the pressure distribution of the airfoils have the minimum pressure peak near the leading edge, followed by a gradual flow deceleration to about the 65%$c$, after which there was a pressure recovery to the trailing edge. The suction peak near the leading edge ensures a reasonable $C_L$ and the gentle adverse pressure gradient which follows destabilizes the laminar boundary layer making it susceptible to transition. The boundary layer on the upper surface of the airfoil stays laminar and attached up to approximately 65%$c$. The entire lower surface is laminar except at large negative angles. The design aims for these airfoil shapes were:

[1] The upper surface contour is designed for the high $C_L$ point of the low drag regime.

[2] The lower surface contour has an undercut near the leading and trailing edge regions and is designed to meet the low $C_L$ limit of the low drag regime.

Boundary layer instability promoting devices or turbulators can be used to minimize the pressure drag caused by the separation bubble. A qualitative evaluation of different devices such as roughness strips, bleed holes, and three dimensional elements is given in [Pfenninger et al. 1988]. These devices should be placed to destabilize the boundary layer by promoting the growth of Tollmien-Schlichting (T-S) instabilities without incurring an unacceptable large device drag penalty. Three dimensional turbulators devices have an advantage over two dimensional turbulators for this as they have greater boundary layer destabilizing capability and a lower device drag. Turbulators located on the front of the airfoil are favorable because they create instabilities but do not disrupt the laminar flow. However, as they are located in a relatively high speed region of the boundary layer, their device drag for a given height is greater than for devices located behind the maximum thickness point.

For low Reynolds numbers [Evangelista & Vemuru 1989] have shown that the Drela airfoil analysis code gives reliable results that compare favorably with experimental data. Some computed predictions for the ASM-LRN-010 airfoil using the Drela code are shown in Figure 3; more details such as the pressure distributions may be found in [Pfenninger et al. 1988]. Predictions for the NASA LRN-1010 are shown in Figure 4. Drag measurements for different $R_c$ for the NASA LRN-1010 are shown in Figure 5a. As the $C_d$ reduces sharply at $\alpha = 5°$, natural boundary layer transition probably occurred preventing the formation of a laminar separation bubble (flow visualization observations indicated that the bubble starts at about 65%c for the $\alpha$ values in the low $C_d$ range). The effects of serrated turbulators for drag reduction are also shown in Figure 5b. The results for the NASA-LRN-1010 using bleed holes and roughness strip turbulators as well as sweep were given in [Siddiqi et al. 1989]. Wind tunnel tests, under the direction of Dr. Pfenninger, were started to evaluate the effect of a single row of suction holes on transition. Suction appears to have a greater drag reduction potential than turbulators even after accounting for the power required for the suction. These experiments were done with another LRN airfoil and the results will be reported when the test series is completed.

The results shown in Figure 5 indicate that the severe laminar separation drag penalties for $150{,}000 < R_c < 400{,}000$ in the $-1° < \alpha < 6°$ range can be reduced by up to 20%. The choice of the turbulator for the wing is perhaps not as critical as that for the canard, which operate at about $R_c$=125,000 for flight at 25 *knots*. The horizontal and vertical tails used NACA 0008 airfoils and, therefore, do not have severe separation bubble penalties at moderate $C_L$'s for low Reynolds numbers.

## IV INDUCED DRAG REDUCTION

A high wing is the obvious choice for minimizing the lift loss (and hence induced drag penalty ) caused by the presence of the fuselage. The RPV was designed to obtain its $\frac{L}{D}|_{max}$ at $25\,knots$, with a $C_L$=1.2 for the wing and fuselage combined. The wing then operates at $R_c$=250,000 with $a$=.092 and $\alpha$=4.5°, its $C_D$ =.012 and $C_{Di}$=.022 assuming an $e$=.95. It should be possible to further reduce the induced drag by improving $e$. Wing tip feathers were designed for this purpose by computing the lifting line vortex wake rollup with an inviscid Point Vortex Method (PVM). For wake rollup, the PVM seems to give more reliable results than a vortex lattice method. This was investigated in [Siddiqi 1987]. Figure 6 shows the computed wake rollup shape for an elliptically loaded lifting line. Figure 7 shows the computed rollup for the wing with two feathers, the front one deployed up at 50° and the rear one downwards at −20°. The $C_{Di}$ of the two wings was compared keeping $C_L$, S, b, and $AR$ the same. The reduction in $C_{Di}$ is seen from the plot of the non-dimensional downwash $W$ on the lifting line. The inboard value for both wings is $W$=1, which means that it is equal to the uniform downwash of an elliptically loaded lifting line, $w_e = \frac{\Gamma_o}{2b}$. As $W$ is less than 1 on the feathers this results in a computed $C_{Di}$ reduction of approximately 10% for the whole wing. Similar induced drag computation studies have been done for swept and crescent wing tips in Germany, by [Eppler 1987] and in the NASA LaRC, by [Vijgen, Dam & Holmes 1989].

Tip feathers were proposed by Pfenninger in Zurich for induced drag reduction in 1943 and hence the use of the term *Pfenninger Pfeathers* by the authors is justified. The use of pfeathers on the wing should give a computed $C_{Di}$=.0198 for $C_L$=1.2. Viscous effects on the pfeathers will increase this value, however, the pressure drag detriment of these effects can be minimized by well designed pfeather junctures. The canard chord was chosen to give a $R_c$=125,000 for $V = 25\,knots$ which means that the friction drag will be $C_D$=.03. The canard $AR$=8 and so for $C_L$=.9 the induced drag is approximately $C_{Di}$=0.036 assuming an $e$=.9. Pfeathers were not considered for the canard because the overall drag penalty of the canard is small since $S_c/S$=.092 giving $C_{Di_c}$=.0033 referenced to the wing area.

The LRN literature suggests that boundary layer separation may be induced on the wing upper surface by the close passage of a vortex wake. The vortex wake rollup computations showed that a low canard position would ensure that its vortex wake passes below the wing for high $\alpha$. The wake centerline position was determined from the vortex wake rollup computations and the viscous wake thickness was added to this centerline using a turbulent boundary layer thickness formula for the upper surface and a laminar boundary layer formula for the lower surface. The horizontal tail was also positioned so that the wing wake passed above it for the high $\alpha$ cases (this was done because the tail is downloaded for this case) and the canard wake passed well below it.

## V STABILITY AND CONTROL

The design specifications require a positive static margin (+SM) RPV which has *good* handling characteristics. A horizontal tail volume factor of .34 (with $S_t/S$=.15) and a vertical tail volume factor of .016 (with a vertical tail area ratio, $S_v/S$=.15) were chosen based on historical data. The selection of canard and tail $c$ and $AR$ requires a careful tradeoff between the friction drag and the induced drag. A canard and horizontal tail of $AR$=8, resulted because their chords were selected to ensure that they fly above a $R_c$ = 125,000 for $V = 25\,knots$ ($c_{c_{avg.}}$ = .5 ft. $b_c$ = 4 ft). The $C_{L\max}$ of the canard is also limited by its aspect ratio limitation. Ensuring good handling qualities is a design challenge closely tied to the RPV's dynamic stability characteristics. The three main handling features that were judged to be desirable were:

[1] Predictable and gentle stall and departure characteristics.

[2] An acceptable flying workload for the pilot.

[3] Uncoupled longitudinal and lateral flight modes.

To ensure slow flight, the configuration should have as high a $C_{Lmax}$ as possible. The nosedown $C_{m_{ac}}$ is usually quite large (-.1 to -.16) for such LRN airfoils; this generally forces the use of a highly downloaded horizontal tail causing a relatively high trim drag penalty for LRN flight. The wing has to compensate for this download which compromises its $C_{L\max}$. A partial solution to this problem with a conventional configuration is to locate the $cg$ aft of the wing $ac$ so that the moment due to $C_L$ compensates for the $C_{Mac}$ at the expense of SM.

The following three configurations were investigated and evaluated based on the above guidelines and on their predicted $\frac{L}{D}$ values.

[1] A conventional tail aft configuration.

[2] A canard configuration.

[3] A three surface configuration.

To get predicted $\frac{L}{D}$ values for each configuration component drag was summed up and a $C_D$ computed. A half-scale model of the original LAURA design was tested in the University of Maryland's wind tunnel. It was a twin boom tail configuration and the results of these tests were reported in [Mangalam et al. 1987]. The $C_L, C_D, \& C_M$ for this wing and fuselage alone are shown in Figure 8. The wing and fuselage $C_{Di}$ is included in the $C_D$. As these tests were done in 1986 the NASA LRN-1010 airfoil was used instead of the ASM-LRN-010. The LRN $C_L \& C_D$ characteristics for the NACA 0008 chosen for the tail airfoils were computed using the Drela Code, and the predictions are shown in Figure 9. The profile drag of the horizontal tail, vertical tail, and canard airfoils was estimated from these computations and wind-tunnel tests. The sectional drag due to elevator and flap deflection was estimated from Figure 3. The induced drag due to the canard and horizontal tail (the *trim* induced drag) was added. The landing gear drag based on wind-tunnel tests was also added (it was half that of the fuselage).

The trim condition for the three surface configuration is calculated as follows. The fuselage angle of attack, $\alpha_{fus}$, is set to give the wing $C_{L_{wing}}$ desired for a flight condition. The trim $C_L$'s for the canard & tail required for $C_{M_{cg}} = 0$ are obtained by calculating their induced $\alpha's$ using the vortex wake rollup code discussed in Section IV. The elevator angle needed to trim is then calculated. A few iterations are required for trim because these induced $\alpha's$ depend on the $C_L$.

The three surface configuration offers some interesting handling features, since trim and control capabilities can be separated. If symmetric LRN airfoils with variable incidences were used for the canard and tail it is possible to take another approach to trim this configuration. The wing $C_L$ as before would be set by the fuselage $\alpha_{fus}$, then the canard and tail $C_L$'s can be independently set to the values obtained by simultaneously solving for the aircraft $C_L = C_{L_c} + C_{L_{wing}} + C_{L_t}$ and for $C_{M_{cg}} = 0$. Still other trim solutions are also possible.

An unusual way to gain efficient high speed flight, when the wing $C_L$ is less than the low $C_L$ limit of the low drag region, is to download the canard and the tail thus forcing the wing $C_L$ back into the low drag region. This will shift the low $C_D$ region of the wing to lower aircraft $C_L's$, and so will give a wider low $C_D$ region than cruise flaps alone would offer for this LRN flight regime. Computed graphs for the use of cruise flaps may be found in [Pfenninger et al. 1988].

A comparison of the stability and control characteristics of the three configurations was made. These evaluations were made with a modified version of the linear Stability & Control code given in [Smetana 1984]. The wind-tunnel data for $C_L$ & $C_D$ shown in Figure 8a was used in the analysis for which the $C_D$ was calculated as described above because the $C_L$ & $C_D$ of the ASM-LRN-010 and the NASA-LRN-1010 airfoils are similar. However, the $C_{m_{ac}}$ of the ASM-LRN-010 is about 13% higher, so the $C_M$ data in Figure 8b was appropriately increased.

The systems and pusher engine gave the fuselage an aft cg (46% of its length). The same wing was used for each configuration and placed so that the resultant cg lay on the wing. For each of the configurations the best possible $\frac{L}{D}$ was sought while attempting to have a SM greater than +10%, which experience has shown is necessary for good handling characteristics at these low speeds. The question then arises which configuration has a lower overall drag? This can be partially answered from the comparative results displayed in Table III where the *us* in the phugoid frequency column means that this mode is unstable. The results of the twin boom configuration are included for comparison. It has good stability characteristics but the excessive parasite drag of the booms forced its rejection.

Configurations which had a *cg* aft of the wing *ac* gave a better $\frac{L}{D}$, because they require less download on the tail, but this gave a lower SM. This forces the choice of *cg's* that are on or ahead of the wing *ac*. These results show that the three surface and the conventional configuration give the highest $\frac{L}{D}$. The aft fuselage *cg* puts the conventional configuration at a disadvantage because the tail arm is reduced. The aft fuselage *cg* favors the three surface configuration because the *cg* can be located slightly ahead of the *ac* since the noseup moment due the canard lift compensates for the large nosedown moment of the LRN wing airfoil. An advantage for the three surface configuration is that it should provide greater low speed capability because the aircraft $C_L$ can be greater than the wing $C_L$ alone.

The SM and trim requirements are in conflict for the canard configuration because of the large nosedown $C_{M_{ac}}$ of the wing. A configuration whose *cg* was on the wing could not achieve a +SM. The results shown in Table III were for a $C_{M_{ac}} = -.1$ wing. This had to be used with $S_c/S = .2$ to get a +SM. The canard configuration was also eliminated because the canard must be made to stall before the wing and this reduces the usable $C_{L\max}$ of the wing

For high $R_c$, the $C_{L\max}$ requirement can be met with flaps but for LRNs the increment in lift, $\Delta C_{L_f}$, is limited by laminar separation. Hence, in effect here the $\Delta C_{L_f}$ is provided by the canard. A flap deflection of +5°

(see Figure 3), gives $\Delta Cl_f = .14$, $\Delta Cd_f = .0012$, and hence causes a $\Delta C_{Di} = .0054$. In contrast the canard gives $\Delta C_L = .1$, $\Delta C_D = .0028$ and a $\Delta C_{Di} = .0033$. As the nosedown moment increment due to the flaps is $\Delta Cm_f = -.041$, this will require an up elevator deflection angle increment of $\Delta\delta_e = -6.5°$, or a tail down lift increment of $\Delta C_{L_t} = -.12$, which can require a tail $\Delta\alpha_t$ of 2° or more. The canard creates a noseup moment increment of $\Delta C_M = .15$; this will require a down elevator angle increment to trim, giving a tail $\Delta C_{L_t}$ that will assist wing lift. The $C_{L_t}$ trim penalty is minimized because it can be designed to be kept close to 0. The main advantage of the three surface configuration over the conventional configuration for LRN flight is this, that is, the canard helps to provide equivalent additional $C_{L_f}$ but without the excessive nosedown pitching moment of the flaps.

The computed longitudinal motion natural frequencies were .55 *Hz* for the short period and .15 *Hz* for the phugoid (unstable). The longitudinal handling problem that will require attention is the stall and departure behavior where the longitudinal and lateral characteristics may couple. The wing will stall at a fuselage angle of approximately $\alpha_{fus} = 10°$. This happens because the wing geometric incidence angle with respect to the fuselage was set to 4°, because the endurance optimization requires a high wing $C_L$. This also means that virtually no take-off rotation will be required as the wing will already be at a high $C_L$ in the take-off roll.

The two lateral stability derivatives were estimated to be $C_{l_\beta} = -.02$ and $C_{n_\beta} = .04$ ( the rolling and yawing moment coefficient changes with respect to $\beta$ ). The twin vertical tails probably only provide a combined effectiveness of approximately 1.5 times that of each vertical tail at these Reynolds numbers. The predicted lateral handling characteristics are that the roll mode will be heavily damped, the Dutch roll lightly damped, while the spiral mode will be unstable.

## VI STRUCTURES & FABRICATION

The design aim was to keep the wing weight below 15 *pounds* so leaving an additional 5 *pounds* for the control surfaces. For such low wing loadings a major structural problem is to ensure stiffness in torsion to prevent skin buckling especially near the root. The wing twist angle, $\theta$, near the tip, can be expressed as, $\theta \sim \frac{n\ W\ AR}{c\ t_{skin}\ G}$ (where $t_{skin}$ is the skin thickness and $G$ is the shear modulus). The main spar was located at 36%*c* and the rear spar at 80%*c* with a styrofoam ( 2 $lb./ft^3$ ) core in between. Even slow and careful hot wire cutting of the foam core requires a filler to cover surface voids which hurt smooth airfoil contour. Instead of time consuming filling, .0156 *inch* wood veneer sheets were bonded to the core. The torsion box was completed by covering this with a layer of .004 *inch* thick fiber glass oriented in the 0° and 90° directions. This compromised the $G$ which would be much higher if the cloth could be layed out at ±45°, but, had to be done in order to avoid skin lap joints as the cloth is typically available in widths of only 45 *inches*. This airfoil contour torsion box was chosen rather than a circular tube to serve as the torsion box and spar because the torsional stiffness is proportional to the square of the enclosed area of the torsion cell.

The wing spar was a bending stiffness design rather than a bending strength design, because the wind tip deflection $\frac{\delta}{b/2} \sim \frac{nW\,AR^2}{c\,E}$, ( where $\delta$ is the tip deflection, $E$ is the modulus of elasticity and $I$ is the moment of inertia of the spar section, and $\frac{\delta}{b/2} \approx \frac{.05\,nW\,(b/2)^2}{E\,I}$ for an elliptically loaded wing). The tip deflection, $\delta$, was designed to be 20% of the semi-span under maximum load. The entire bending load is taken by the I-beam main spar which has high modulus uni-directional carbon fiber caps (estimated to be 43% of the wing weight). The shear web was a single layer of fiber glass sandwiched between end grain balsa wood. Wing taper was achieved by a swept forward trailing edge while the leading edge of the wing was kept straight. The main spar was then swept forward relative to the wing so that the wing aerodynamic loads would twist the tips nosedown compared to the inboard sections. This flexible structure will give a dihedral angle that increases with $g$ loading. Static testing of the wing alone under load ( 4.25 $g$'s) verified the structural design and the tip deflection was within 10% of the predicted value.

The MIT Dadelus experience related in [Cruz & Drela 1990] showed there can be a significant forward-bending load for such high aspect ratio wings when flying at high $C_L$'s. The lift vector then can have a large component in forward direction, especially near the tips, which causes this bending load. The rectangular section balsa wood rear spar was strengthened with a layer of uni-directional carbon fiber along its rear face to provide stiffness to handle the tension load imposed by this forward bending.

The majority of the wing weight is then in the primary structure (estimated to be 80% of the total wing weight). The original RPV was to have a gross weight of 45 *pounds*. However, for flight testing, the on-board telemetry and measurement systems increased the fuselage weight by about 11 *pounds*. The RPV gross weight is now therefore 56 *pounds*, its flight envelope will be limited to 3.5 *g's*.

The canard has a taper ratio of .6 and was built using a female mold as it is difficult to contour the NASA-LRN-1010 airfoil accurately for small chords by hot wire cutting of foam. The canard main spar, like that of the wing, was also constructed of carbon fiber and balsa wood and its rear spar was also made of balsa wood, but its skin was not supported by a solid foam core. A .0625 *inch* balsa wood sheet was sandwiched between two layers of .004 *inch* fiber glass cloth to form the skin. The fiber glass for the skin was oriented along the ±45° directions to maximize $G$ and hence the torsional stiffness. It was equipped with full span trailing edge cruise flaps.

The horizontal and vertical tails were built using typical model aircraft construction techniques. The spars, ribs, and skin were made of balsa wood and then covered with a layer of Monokote. The wing, canard, and tails were all equipped with solid balsa wood control surfaces that started aft of the 80%c rear spar location. These surfaces were additionally strengthened with a single layer of fiber glass or carbon as judged necessary. The control surfaces were all attached to the rear spar by means of plastic hinges that were inserted into cutouts in the rear spar and the control surfaces. The wing control surfaces were split into three sections each run by its own servo motor to provide redundancy or fault tolerant controls. The innermost controls functioned as cruise flaps and the two outboard control surfaces as ailerons and cruise flaps. Similarly the horizontal and vertical tail elevators and rudders were also split and run by independent servo motors. The canard flaps and the elevators were linked for pitch control via electronic mixing functions available in the radio control equipment (a Futaba PCM system).

The weights of the components built were:

Wing Wt.: 14 pounds.
Canard Wt.: 1.25 pounds.
Horizontal tail Wt.: 1.5 pounds.
Vertical tails Wt.: 1.8 pounds.

## VII FLIGHT TESTING

Currently, captive ground tests are being done with the RPV mounted on a truss fixed to the front of a truck. The test fixture gimbals allow freedom of motion in the pitch and yaw but not in roll. These tests indicated that the the RPV had acceptable stall and departure characteristics and demonstrated pitchdown control when stalled nose high. The flight tests will be challenging as they have to verify the performance predictions in the presence of aeroelastic and wind gust effects on the large $\mathcal{R}$ wing.

## ACKNOWLEDGEMENT

This work was partially funded under NASA contract NAS1-18599. The authors would like to thank their NASA LaRC sponsor Mr. W. D. Harvey, for his project management support. We are grateful to the Computational Fluid Dynamics Lab. of NASA LaRC for the use of its computing facilities. We would like to express our gratitude to Mr. R. Foch and Ms. P. Toot, of the NRL, for their support, technical advice and comments during the course of this design effort.

## REFERENCES

(1) B. H. Carmichael, Low Reynolds Number Airfoil Survey, NASA CR 165803, V1 Nov 1981.

(2) J. R. Cruz, M. Drela, Structural Design Conditions for Human Powered Aircraft, Technical Soaring, V14, N1, 1990.

(3) R. Eppeler, Die Entwicklung der Tragflugeltheorie, Z. F. W., V11 (1987).

(4) R. Evangelista, C. S. Vemuru, Evaluation of an Analysis Method for Low-Speed Airfoils by Comparison with Wind Tunnel Results, AIAA 89-0266, 27th Aero. Sc. Meet., Reno, Nevada, Jan 1989.

(5) R. Evangelista, et al., Design and Wind Tunnel Test of High Performance Low Reynolds Number Airfoil, AIAA-87-2349-CP, AIAA 5th Appl. Aero. Conf., Monterrey, Calif., Sept 1987.

(6) R. Evangelista, Design and Evaluation of a Low Reynolds Number Airfoil, M.S. Thesis, George Washington University 1987.

(7) J. C. Ferris, R. J. McGhee, R. W. Barnwell, Low-Speed Wind-Tunnel Results for Symmetrical NASA LS(1)-0013 Airfoil, NASA TM 4003, Aug 1987.

(8) R. J. Foch, R. E. Wyatt, Low Altitude/Airspeed Unmanned Research Aircraft (LAURA) Preliminary Development, Int. Conf. on Aerodynamics at Low Reynolds Numbers, UK, 1986.

(9) R. J. Foch, Detailed Technical Specifications for the Low Altitude/ Airspeed Unmanned Research Aircraft, U.S. Naval Research Laboratory, Washington, D.C. 1986.

(10) K. A. Jacob, B. S. Rangashayi, J. Jayaraman, R. Peravali, Some Fabrication Experiments towards a Composite RPV Wing, Proc., 4th Int. RPV Conf., Roy. Aero. Soc. & Univ. of Bristol, Apr 1984.

(11) C. L. Ladson, Effects of Independent Variation of Mach & Reynolds Numbers on the Low-Speed

Aerodynamic Characteristics of the NACA 0012 Airfoil Section, NASA TM-4074, Oct 1988.

(12) S. M. Mangalam, W. D. Harvey, S. Siddiqi, Development of Wing and Tail Configurations for Low Altitude Unmanned Research Aircraft, SAE 871882, Aero. Tech. Conf. & Expo., Long Beach, Calif., Oct 1987.

(13) S. M. Mangalam, et al., Transition and Separation Control on a Low Reynolds Number Airfoil, Int. Conf. on Aerodynamics at Low Reynolds Numbers, London, UK 1986.

(14) S. M. Mangalam, W. Pfenninger, Wind-Tunnel Tests on a High Performance Low-Reynolds Number Airfoil, AIAA-84-0628, AIAA 13th Aerodynamic Testing Conf., Mar 1984.

(15) M. D. Maughmer, D. M. Somers, Figures of Merit for Airfoil/Aircraft Design Integration, AIAA-88-4416, AIAA/AHS/ASEE, A/C Design Sys & Ops Meet, Atlanta, Ga., Sept 1988.

(16) R. J. McGhee, B. S. Walker, B. F. Millard, Experimental Results for the Eppler 387 Airfoil at Low Reynold Numbers in the Langley Low-Turbulence Pressure Tunnel, NASA TM 4062, Oct 1988.

(17) M. M. O'Meara, T. J. Mueller, Laminar Separation Bubble Characteristics on an Airfoil at Low Reynolds Numbers, AIAA J., V25, N8, Aug 1987.

(18) T. J. Mueller, Low Reynolds Number Vehicles, AGARDograph No. 288, 1985.

(19) W. Pfenninger, C. S. Vemuru, Design of Low Reynolds Number Airfoils-I, AIAA-88-2572, AIAA 6th Appl. Aero. Conf., Williamsburg, Virginia, Jun 1988.

(20) W. Pfenninger, C. S. Vemuru, S. Mangalam, R. Evangelista, Design of Low Reynolds Number Airfoils-II, AIAA/ASME/SIAM/APS-88-3764-CP, 1st Nat. Fluid Dyn. Cong., Cincinnati, Ohio, Jul 1988.

(21) W. Pfenninger, Investigation on Reduction of Friction on Wings in Particular by Mean of Boundary Layer Suction, NASA TM-1181, 1947.

(22) W. Pfenninger, Experimental Investigation of an Airfoil with High Lift-to-Drag Ratios at Low Reynolds Numbers, Northrop BLC Report 84 (NAI 560188) 1956.

(23) M. S. Selig, J. F. Donovan, D. B. Fraser, Airfoils at Low Speeds, Soartech 8, 1989, H. A. Stokely Publisher, Virginia Beach, Virginia.

(24) S. Siddiqi, Trailing Vortex Rollup Computations Using The Point Vortex Method, AIAA-87-2479-CP, Proc. 5th AIAA Appl. Aero. Meet, Monterey, Calif., Aug 1987.

(25) S. Siddiqi, T. S. Kwa, R. Evangelista, The Design of a Low Reynolds Number RPV, Proc. of the Low Reynolds Number Conf., Springer-Verlag, Heidelberg, Germany, 1989.

(26) F. O. Smetana, Computer Assisted Analysis of Aircraft Performance Stability & Control, McGraw-Hill Book Co., New York 1984.

(27) J. L. Stollery, D. J. Dyer, The Flight Performance of an RPV Compared with Wind Tunnel and Theoretical (CFD) Results, ICAS-88-4.9.2, p1392, Proc. 16th Cong. of the Int. Council of Aero. Sc., Jerusalem, Israel, 1988.

(28) T. Vranas, Mold and Model Making Techniques, NASA Langley Research Center, 1984.

(29) P. M. H. W. Vijgen, C. P. van Dam, B. J. Holmes, Sheared Wing-tip Aerodynamics: Wind Tunnel & Computational Investigation, J. of Airc., V26, N3, 1989.

## TABLE I AIRCRAFT DESIGN SPECIFICATIONS

| | |
|---|---|
| Gross Wt.: 56 lb. | Airfoil: ASM-LRN-010 |
| Wing & Control Surf Wt.: 20 lb. | Airfoil $t/c$ 9.5% |
| Ult. Load Factor: +4.5 -3 g's | Mean Geom. Chord: .98 ft. |
| Speed: 25 - 50 knots | Wing Span: 22.2 ft. |
| Min. ROC Gross Wt.: 400 fpm | Wing Area: 22.09 ft.$^2$ |
| Fuselage Length: 6.67 ft. | $AR$ = 22. |
| Stick Fixed Static Stab. Required | Taper Ratio: .6 |
| Flutter Speed > 90 knots | Max. Power SL: 3.1 HP |

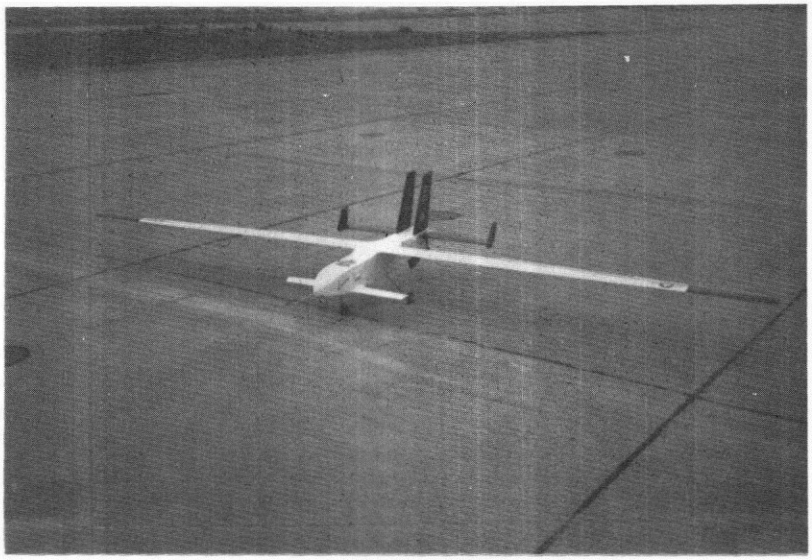

Fig 1. The NASA/AS&M RPV without Tip Pfeathers

Drela code predictions $R_c$=250,000

$C_l/C_d$=115 @ $C_l$=1.26, $C_{mac}$=-.16

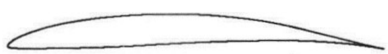

Fig. 2. The ASM LRN-010 airfoil

## TABLE II LRN AIRFOIL FIGURE OF MERIT COMPARISONS

| WIND TUNNEL DATA | $FOM_e$ | COMPUTATION | $FOM_e$ |
|---|---|---|---|
| **NASA LRN-1010** $R_c$=250,000 | **110** | **ASM LRN-010** Drela Code $R_c$=250,000 | **115** |
| **Eppler 387** [McGhee 1988] $R_c$=300,000 | **100** | **NACA 0010 Drela Code** $R_c$=250,000 | **54** |
| **Wortmann FX63-137** [Stollery 1988] $R_c$=300,000 | **60** | | |

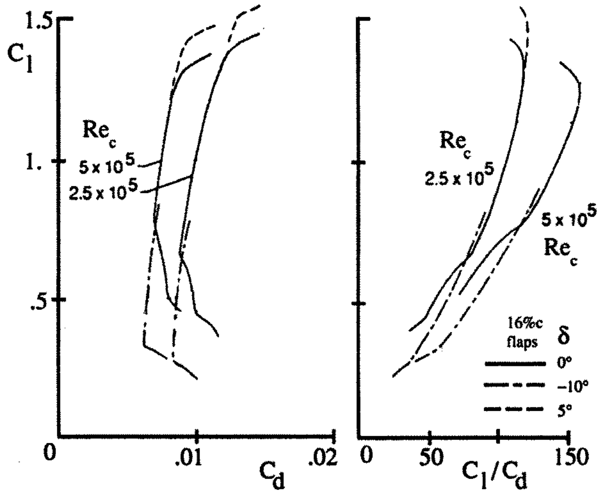


Fig. 3. ASM-LRN-010 Airfoil Characteristics

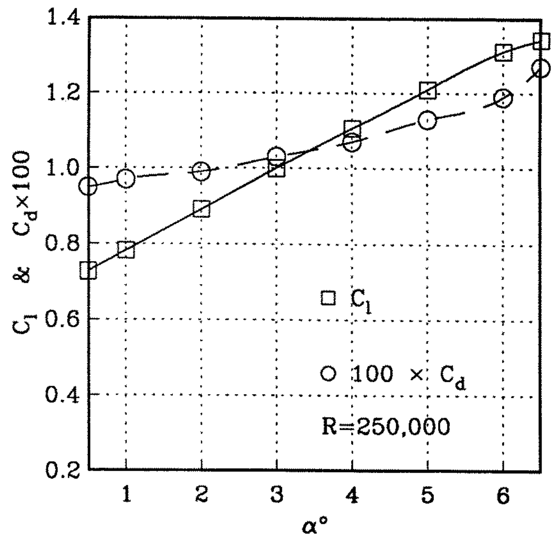


Fig. 4. LRN−1010, Drela Code n=9

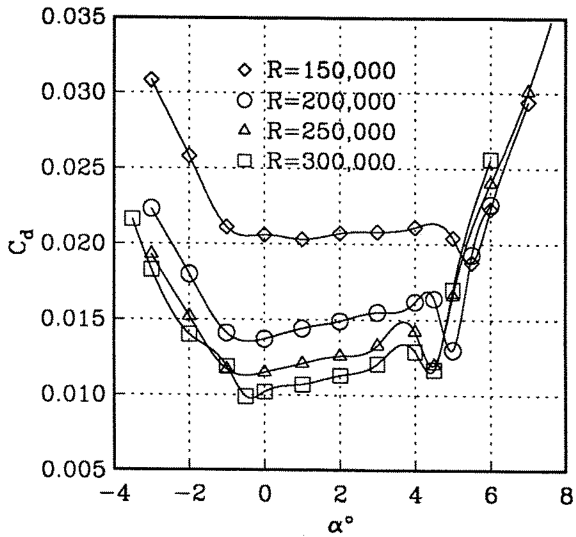


Fig. 5a. LRN−1010 $C_d$ v/s α

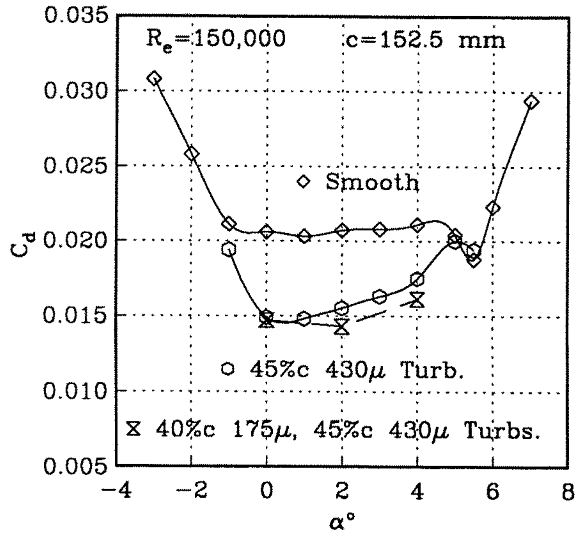


Fig. 5b. LRN−1010 Turbulator Tests

Fig. 6. Elliptic Lift Wake Vortex Rollup

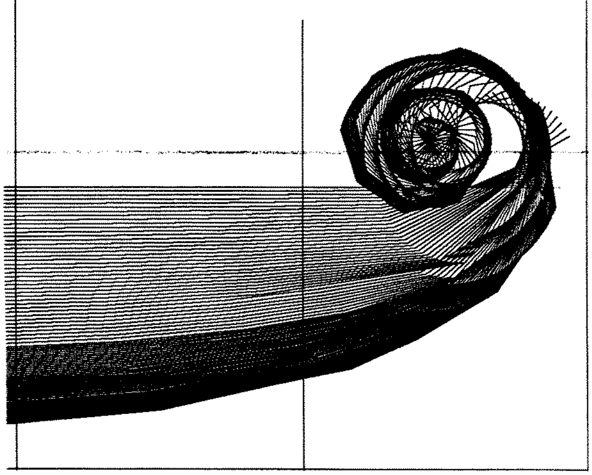

Fig. 7 Elliptic Lift Vortex Rollup, .125s Pfeathers +50° & -20°.

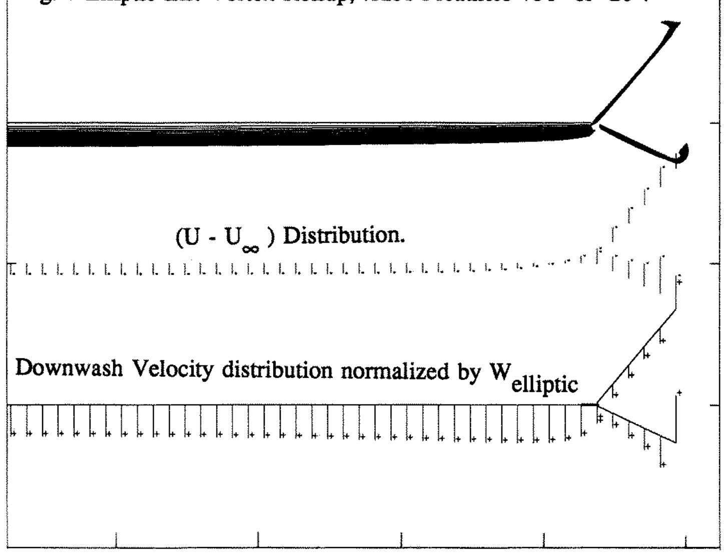

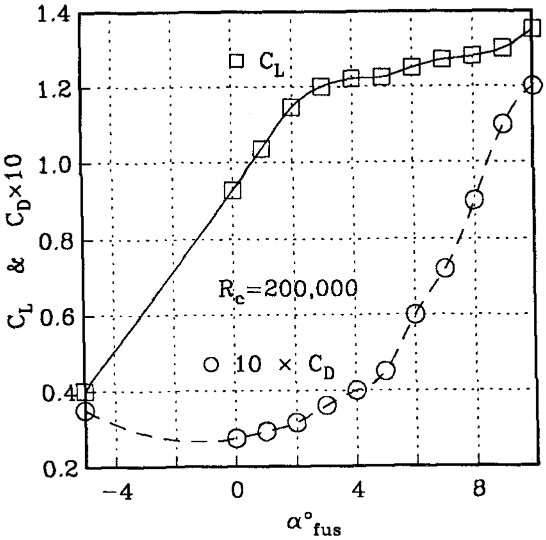

Fig. 8a. 1/2 Scale RPV Wing & Fus.

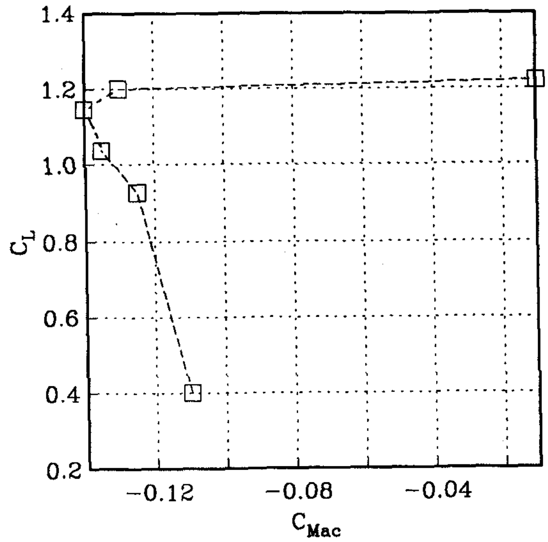

Fig. 8b. 1/2 Scale RPV Wing & Fus.

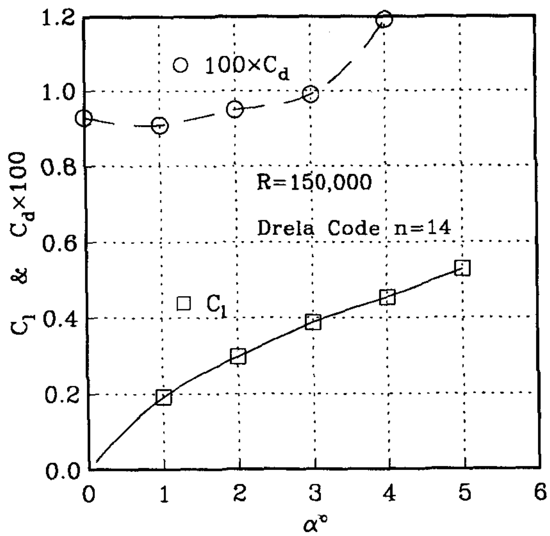

Fig. 9. NACA 0008

**TABLE III CONFIGURATION COMPARISONS & LONGITUDINAL STABILITY**

| Configuration | V | $\frac{L}{D}$ | SM | $C_L$ | $C_{L_c}$ | $C_{L_w}$ | $C_{L_t}$ | $\omega_{n\,sp}$ | $\omega_{n\,ph}$ |
|---|---|---|---|---|---|---|---|---|---|
| Twin Boom | 26 | 19.5 | .2 | 1.14 | - | 1.14 | 0.3 | 3.75 | .73 |
| Conventional | 25 | 25. | .16 | 1.205 | - | 1.24 | -.35 | 3.36 | .94 us |
| Canard | 25 | 18. | .06 | 1.205 | 1.1 | .97 | - | 2.55 | .75 us |
| 3 Surface | 25 | 25. | .15 | 1.205 | 1.03 | 1.16 | -.3 | 3.4 | .92 us |